

8-5-1989

Collection of Backscattered Electrons with a Single Polepiece Lens and a Multiple Detector

I. Müllerová

Czechoslovak Academy of Sciences

M. Lenc

Czechoslovak Academy of Sciences

M. Florián

Tesla Brno

Follow this and additional works at: <https://digitalcommons.usu.edu/microscopy>



Part of the [Life Sciences Commons](#)

Recommended Citation

Müllerová, I.; Lenc, M.; and Florián, M. (1989) "Collection of Backscattered Electrons with a Single Polepiece Lens and a Multiple Detector," *Scanning Microscopy*: Vol. 3 : No. 2 , Article 3.

Available at: <https://digitalcommons.usu.edu/microscopy/vol3/iss2/3>

This Article is brought to you for free and open access by the Western Dairy Center at DigitalCommons@USU. It has been accepted for inclusion in Scanning Microscopy by an authorized administrator of DigitalCommons@USU. For more information, please contact digitalcommons@usu.edu.



COLLECTION OF BACKSCATTERED ELECTRONS WITH A SINGLE POLEPIECE LENS
AND A MULTIPLE DETECTOR

I. Müllerová*, M. Lenc and M. Florián¹

Institute of Scientific Instruments, Czechoslovak Academy of
Sciences, 612 64 Brno, Czechoslovakia
¹ Tesla Brno, Czechoslovakia

(Received for publication March 06, 1989, and in revised form August 05, 1989)

Abstract

This paper is a part of a study on the use of a single-polepiece lens as an objective lens of an analytical scanning electron microscope (SEM). The single-polepiece lens has proved to be very suitable for the efficient collection of backscattered electrons (BSE) with a multi-element semiconductor detector. For the BSE images in the sum and difference modes the contrast is a non-monotonic function of the excitation of the lens, due to the complicated nature of the BSE trajectories. The use of a six-element semiconductor detector provides a whole variety of BSE signal compositions in the conventional SEM as well as in a SEM with a single-polepiece lens.

KEY WORDS: Single-polepiece lens, Backscattered electron trajectories, Multielement semiconductor detector, Backscattered electron image contrast.

*
Address for correspondence:
I. Müllerová

Institute of Scientific Instruments, Czechoslovak
Academy of Sciences, 612 64 Brno, Czechoslovakia
Phone: 42 - 5 - 749292

Introduction

Many different types of BSE and secondary electron (SE) detectors have been designed and tested to make the signals more and more quantitative. BSE detectors make use of straight line trajectories, so it is not possible to detect all BSE if we desire to have some free space above the specimen (e.g. for other detectors). Then the BSE strike all detectors around the specimen (e.g. SE detector, X-ray detector) and the specimen chamber walls. The complicated distribution of the currents in a specimen chamber was described by Oatley (1983). These currents can cause some additional problems when e.g. EBIC and EBIV signals are measured. To get a pure signal of the one type some special mixing of several different signals is necessary (Reimer and Riepenhausen, 1985).

The disadvantage of the classical arrangement of the SEM led us to the use of a single-polepiece lens (Mulvey, 1985) with the specimen immersed in the strong magnetic field. This enabled us to obtain trajectories of BSE and SE. It is desirable that no parasitic electrons strike the detectors above the specimen or be incident back onto the specimen.

The single-polepiece lens as a scanning electron microscope objective was first used by Hill and Smith (1982). They investigated the effects of the magnetic field of the lens on the secondary and backscattered electrons and studied some electron optical parameters, especially low chromatic (4.4 mm) and spherical aberration (2.2 mm) coefficients.

Bode and Reimer (1985) used a single-polepiece lens for the detailed study of the BSE signals. They pointed out the advantage of the low spherical aberration of the single-polepiece lens and presented photographs obtained using the sum signal mode which showed decreased topographic contrast and photographs obtained using the difference signal mode which showed decreased material contrast. They discussed the advantages and disadvantages of detector strategy of the different signal modes making use of the specific properties of this lens.

The single-polepiece lens is not used in any commercial instrument. The Hitachi SEM S-570

takes advantage of the configuration with the specimen immersed in the strong magnetic field.

We are concerned with the possibilities of the detection of BSE using a multiple semiconductor detector in a SEM with a single-polepiece lens. Recently we have used the three-segment detector for colour imaging with BSE (submitted for publication in Scanning). In that paper we further try to answer the question, whether an odd number of detectors enables the standard imaging with sum and difference signal modes common for an even number of detectors. We have arrived at a positive answer both theoretically and experimentally for the classical arrangement in SEM. Our first results concerning the detection of BSE with the single-polepiece lens were presented at EUREM 88 (Lenc and Müllerová, 1988).

In the present paper comparison of the BSE signals detected by the six segment semiconductor detector in the classical arrangement and by that in the arrangement using a single-polepiece lens is made. Special attention is paid to the sum and difference signal modes in both arrangements.

Detection of BSE with the classical arrangement

All our experiments were performed in the BS 350 UHV SEM (Delong et al. 1978) with our new six-segment semiconductor detector (Fig.1). This

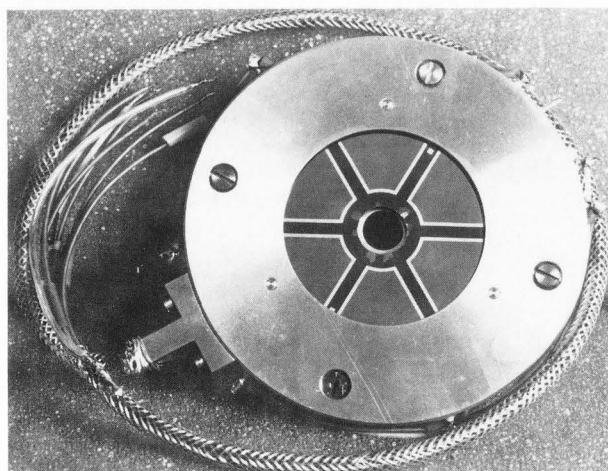


Fig. 1: Multisegment semiconductor detector with six PIN diodes. The inner radius of the active area is 6 mm, the outer radius is 16 mm.

detector consists of six PIN diodes in one chip, each of them having an active area of 100 mm² and a capacity of about 600 pF. We aimed to have an area of this detector as large as possible which would, however, still allow us to work with TV frequency without any reverse bias. The six segments are used to provide the possibilities of working with odd and even numbers of detectors

and small and high collection solid angles. The dimensions of the detector and its position are given in Fig.2. As a specimen a sphere of 600 μm

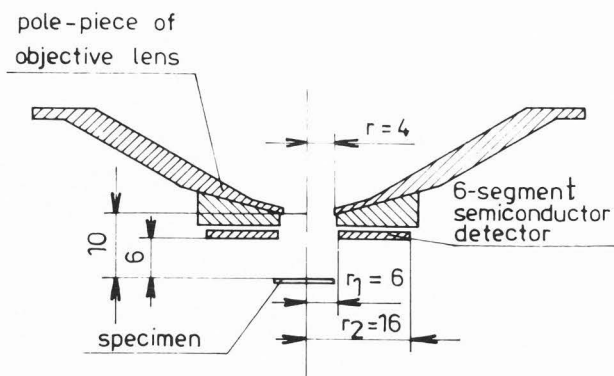


Fig. 2: Position of the semiconductor detector above the specimen and below the lower polepiece of the objective lens in the classical experimental arrangement.

diameter covered by a thin gold layer on a carbon substrate is used. The sum signal of backscattered electrons from all six segments and the line scan along the central x-line is shown in Fig.3. The large solid angle difference signal of backscattered electrons (sum of signals of three segments minus the sum of signals of three opposite segments) with a line scan along the central x-line is shown in Fig.4. This agrees well with the results presented by Hejna and Reimer (1987) and Reimer et al. (1984). Our photographs were taken with a primary beam energy of 15 keV.

Single-polepiece lens

The experimental set up with the single-polepiece lens is shown in Fig. 5. The calculated axial flux density distribution $B(z)$ for 700 ampere-turns is shown in Fig.6 and the calculated important electron optical parameters are summarized in Table 1. In Fig.6 the positions of the specimen and detector are shown at distances z_1 and z_2 from the polepiece, respectively. To confine the magnetic flux of the single-polepiece lens, magnetic shielding was used. The axial flux density at a distance $z=100$ mm from the polepiece falls to about one thousandth of the maximum flux density, which is a convenient value for the detection of the SE. In our case, the maximum value of the field is about $B_{max} = 0.052$ T for 1 A excitation current (1070 turns were used). For normal operation up to an excitation corresponding to $B_{max} = 0.2$ T no cooling was necessary; for higher values the coil casing was water cooled.

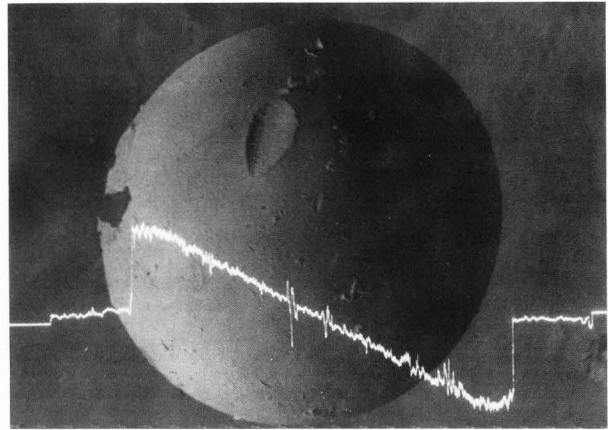
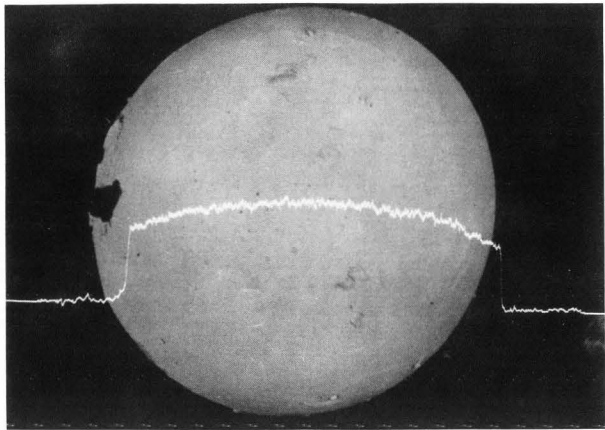


Fig. 3: BSE image in the sum mode of a sphere covered by a thin gold layer on a carbon substrate. The diameter of the sphere is $600\ \mu\text{m}$, primary beam energy is 15 keV. The line scan profile along the central x-line is superimposed. The positions of the detector and the specimen are given in Fig.2.

Fig. 4: BSE image in the difference mode of the same specimen and under the same conditions as in Fig.3. (The line scan is inverted.)

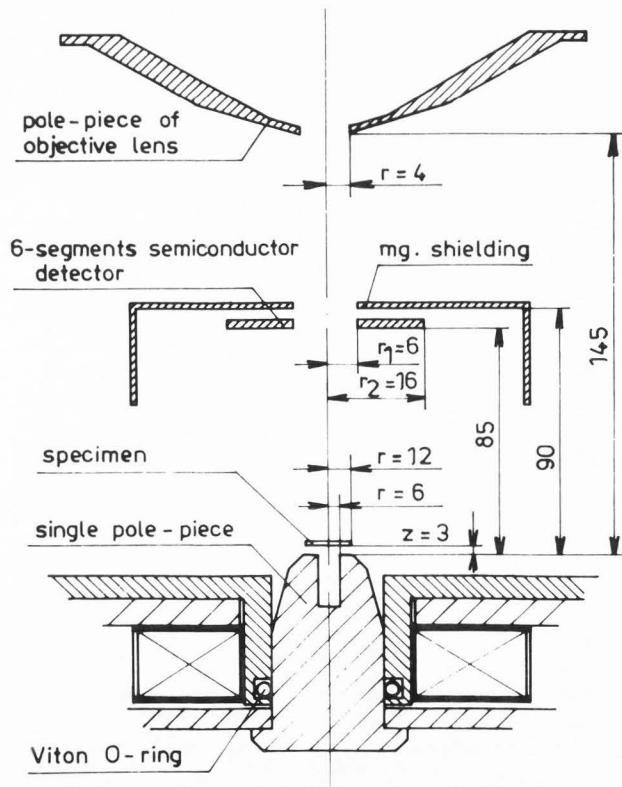


Fig. 5: Experimental arrangement with a single-polepiece lens and a multisegment detector.

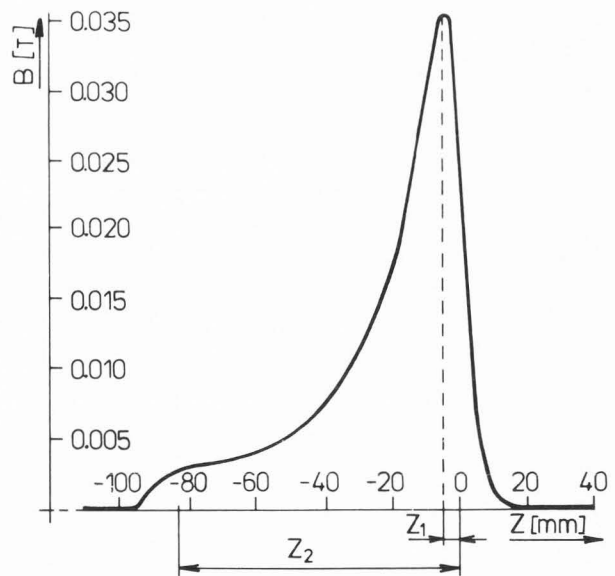


Fig. 6: Computed axial flux density distribution of the single-polepiece lens for 700 ampere-turns. z_1 and z_2 are the coordinates of the specimen and the detector, respectively.

Table 1: Electron optical parameters for single-polepiece lens with the flux density of Fig.6, object at infinity, image at the specimen plane $z_1 = 3$ mm above the top of the polepiece: n is the number of intermediate images, $NI/\sqrt{V_r}$ is the excitation parameter in A/\sqrt{V} , f, C_s, C_c are focal length, spherical and chromatic aberration coefficients in mm.

n	$NI/\sqrt{V_r}$	f	C_s	C_c
0	15.8	19.5	5.4	11.5
1	34.2	-15.2	6.5	12.6
2	53.1	11.7	7.1	13.2
3	72.9	-8.6	7.0	12.8

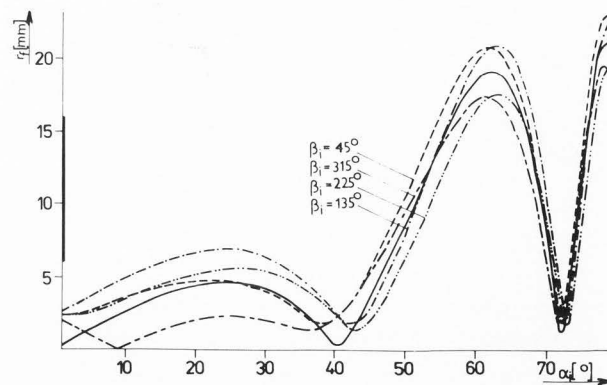
Detection of BSE with the single-polepiece lens

The SE and BSE are guided away by the same magnetic field that focuses the primary beam electrons onto the specimen. The character of the trajectories of the secondary electrons (with a typical energy of the order of electronvolts) in the single-polepiece lens is the same as in other designs, where the electrons originate in the high flux density region (see e.g. Kruit and Dubbeldam, 1987).

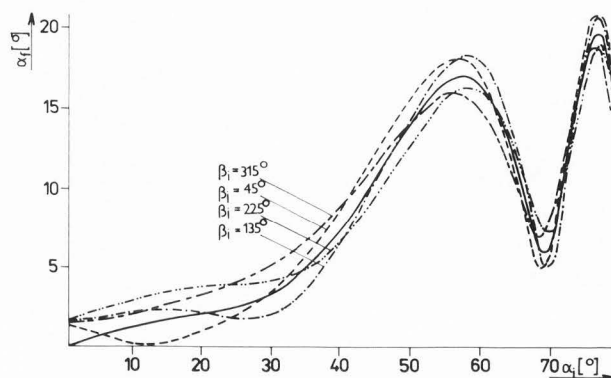
The study of the trajectories of the BSE is a complicated matter. First we must consider the strong non-paraxial character of the trajectories. The directions of the initial velocities vary from 0° to 90° with respect to the optical axis. Then we must consider the broad backscattered electron energy spectrum which contains all energies up to the primary beam energy. Especially for light elements, the spectrum is quite flat; for heavier elements more pronounced maxima exist near the primary beam energy. We cannot expect the parallelization effect for BSE as occurs for SE, because the typical energy of BSE is higher by several orders so that an extremely strong magnetic field would be necessary.

To perform the calculation of the exact BSE trajectories we fitted the calculated axial flux density distribution to Glaser's axial field and then extended this Glaser's field analytically to the whole space. In this way we obtained an analytical expression for the magnetic Lorentz force which was very important for the fast numerical solution of the Newton equation of motion.

First we calculated many trajectories to find a possible relationship between the initial characteristics of BSE, radial coordinate r_i , (for azimuthal angle we put $\psi_i=0$) and the vector of the initial velocity (given by the polar angle α_i , and the azimuthal angle β_i) and the final radial and azimuthal coordinates r_f , and ψ_f , respectively, and the vector of the final velocity given by α_f, β_f, r_f and α_f , as function of α_i for several values of the parameters β_i are plotted in Fig.7a and Fig.7b. r_f and ψ_f as



(a)



(b)

Fig. 7: Calculated dependence of the radial position r_f (a) and the slope α_f (b) of the electron trajectory in the detector plane on the initial slope α_i (polar angle of the velocity vector) for different orientations β_i (azimuthal angle of the velocity vector). The solid line in (a) marks the radial position of the detector.

functions of β_i for several values of the parameter α_i are shown in Fig.8a and Fig.8b. The dashed curves represent the initial radial coordinate $r_i = 0.5$ mm and the full curves stand for electrons originating on the optical axis ($r_i = 0$, there is of course no β_i dependence of α_f and r_f). Thick lines in Fig.7a and Fig.8a denote the radial position of the detector. All curves were calculated with the specimen positioned at $z_1 = 3$ mm and with the detector positioned at $z_2 = 83$ mm; the value of the flux density at maximum $B_{\max} = 0.18$ T and the energy was 15 keV.

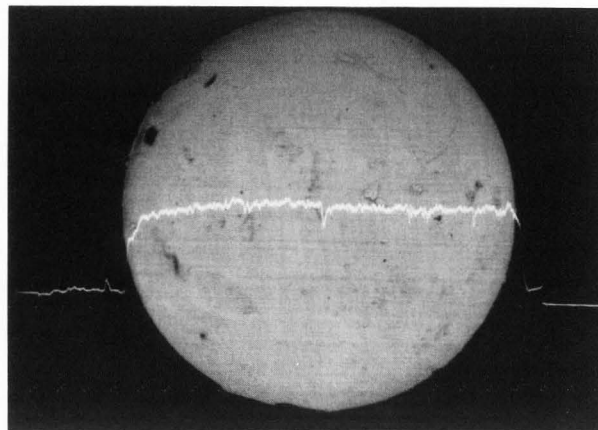
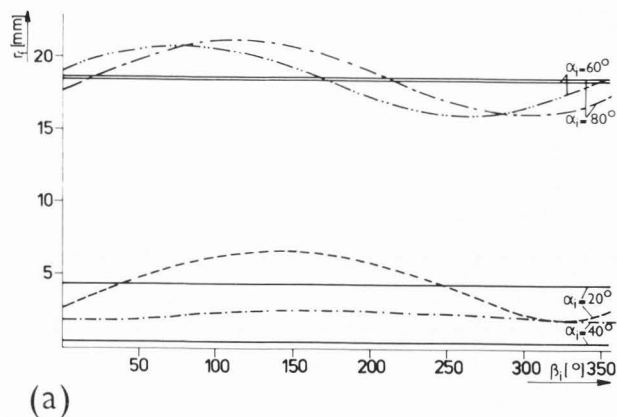


Fig. 9: BSE image in the sum mode of a sphere covered by a thin gold layer on a carbon substrate. The diameter of the sphere is $600 \mu\text{m}$, primary beam energy is 15 keV, the excitation of the single-polepiece lens is 3660 ampereturns. The positions of the detector and the specimen are given in Fig.5. The line scan profile along the central x-line is superimposed.

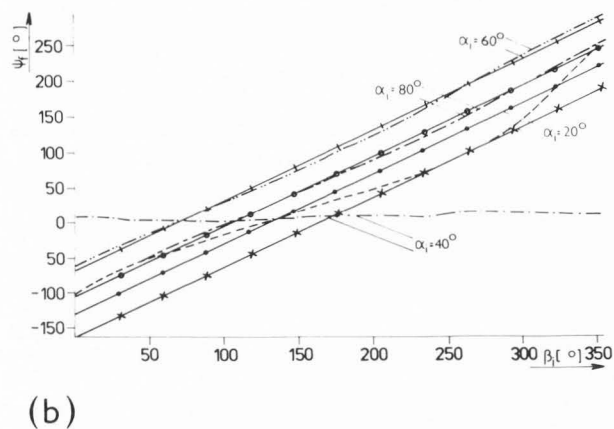


Fig. 8: Calculated dependencies of the radial position r_f (a) and azimuthal position ψ_f (b) of the electron trajectory in the detector plane on the initial orientation β_i (azimuthal angle of the velocity vector) for different initial slopes α_i . The solid line in (a) marks radial position of the detector.

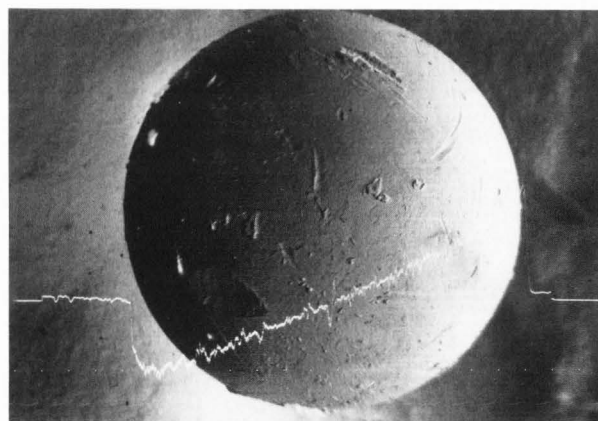


Fig. 10: BSE image in the difference mode for the same specimen and under the same conditions as in Fig.9.

Results

A comparison of the BSE signal from the same specimen detected by the same detector in the classical SEM arrangement and in the set-up with the single-polepiece lens is of considerable interest.

Fig.9 and Fig.10 show micrographs of the same specimen formed in the same way as in Fig.3 and Fig.4, respectively, but now the backscattered electrons originate within the magnetic field. The excitation current of the single-polepiece

lens was 3.42 A; consequently the specimen was situated near the maximum of the flux density $B_{\text{max}} = 0.178$ T. The primary beam energy was again 15 keV and a second image of the crossover was formed in the single-polepiece lens.

For the theoretical comparison we will

define the sum mode as the BSE signal from all six segments of our detector and the difference mode as the sum of the BSE signal from the three segments in the halfplane ($x > 0$) minus the sum of the BSE signal from the three opposite segments in the halfplane ($x < 0$).

For the calculations we integrated eq.(4) of the appendix with the conditions 1 and 2 defined there, and with the energy distribution function for gold ($\eta_0 = 0.49$, $\epsilon_m = 0.97$).

First the relative signal N_r (i.e. the ratio of the detected signal in the sum or the difference modes to the signal which would be detected in the entire halfspace) was calculated as a function of the flux density to study the optimum excitation of the single-polepiece lens for the detection of BSE. The dependencies for the sum and the difference modes (full and dashed lines) are plotted in Fig.11. The curves

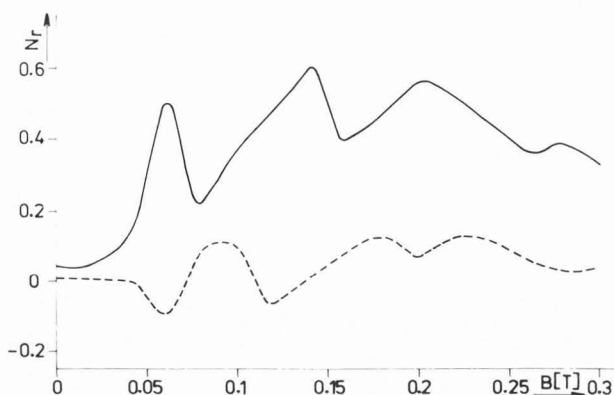


Fig. 11: Calculated dependence of the sum and the difference signals on the excitation of the single-polepiece lens (represented by the maximum value of the axial flux density).

are calculated for a point on the optical axis for the specimen tilted 15° about the y-axis. We measured these dependencies too, and the experimental curves agree well with the calculated ones.

In Fig.3 and Fig.4 the line scan profiles are plotted along the central x-line and they can be compared with the corresponding profiles in Fig. 9 and Fig.10. The calculated curves are shown in Fig.12 and Fig. 13. In Fig.12 there are dependencies of the BSE signal N per one electron with the energy E_d impinging onto the specimen in the sum and difference modes (full and dashed lines) as functions of the position x on the sphere, for $B_{\max} = 0.180$ T. Fig.13 shows the same dependencies for zero flux density and the classical arrangement according to Fig.2.

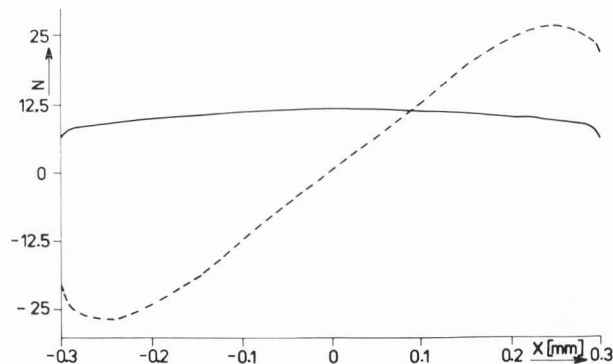


Fig. 12: Calculated line scan profiles for the single-polepiece lens arrangement (Fig.5) (maximum flux density B_{\max} is 0.180 T). Compare with those obtained experimentally (Fig.9 and 10).

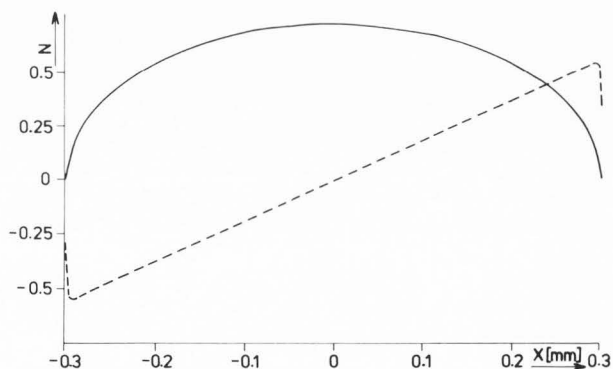


Fig. 13: Calculated line scan profiles for the conventional arrangement (Fig.2). Compare with those obtained experimentally (Fig.3 and 4).

Conclusion

The single-polepiece lens as a scanning electron microscope objective lens offers several new interesting properties. It is shown in Table 1, that the aberration coefficients are low and increase only slightly with an increasing number of intermediate images in the lens. This will be very important in the application of the parallelizing action of the decreasing flux density

on SE or low energy BSE in an analytical microscope with a low primary beam energy.

The large free space above the specimen can be used e.g. for a windowless X-ray energy dispersive detector or an ion beam gun or for the optimum position of the in-lens deflection coils.

In the present paper the BSE signals in the single-polepiece lens were studied. It is evident now, that the non-paraxial character of the BSE trajectories is very important. As an example, for all trajectories in Fig.7b and Fig.8b only those with a large influence of 3rd order spherical aberration intersect the detector surface. The boundaries between low and high take-off angle detectors and between large and small solid angle detectors are smoothed. The BSE trajectories in the magnetic field are functions of the energy. Nevertheless, on the whole (i.e. taking both the energy distribution of the BSE and the energy sensitivity of the detector into account) there are quite interesting dependencies of the sum and the difference signals on the excitation of the single-polepiece lens (see Fig.11). In the present experimental arrangement it is possible, in the sum mode, to get 60% of the total signal at a particular excitation of the lens, and it is also possible, in the difference mode, to get zero at some other excitation of the lens. It is therefore desirable in the future to add an auxiliary lens to the optical system to have the independent possibility of adjusting the single-polepiece lens excitation for BSE detection and for the focusing of the primary beam onto the specimen plane.

We expect that a modification of the idea of a variable axis lens (VAIL) can be employed in a set-up with the single-polepiece lens. There is enough space for the necessary in-lens coils (there are serious UHV design problems, of course), and with the proper adjustment of the predeflection and the in-lens deflection e.g. very broad range of angles of incidence for the primary beam can be obtained.

Appendix

A knowledge of the relationship between the position of BSE in the specimen plane and in the detector plane is necessary, but not sufficient for the study of the contrast (the contrast mechanism in the backscattered electron image is discussed by Robinson, 1980). As is well known, the number of the BSE emitted per second into an elementary solid angle with energy between E and $E + dE$ is given by

$$dN(\epsilon, \alpha_i, \beta_i) = \frac{I_p}{e\pi} F(\epsilon) \cos\Omega \sin\alpha_i d\alpha_i d\beta_i d\epsilon \quad (1)$$

where I_p is the primary beam current, e is the elementary charge, $F(\epsilon)$ is the energy distribution function for BSE, $\epsilon = E/E_p$ is the relative energy of BSE with respect to the primary beam energy E_p , $\cos\Omega$ is the function expressing Lambert's law (Reimer et al. 1984), where Ω is the angle between the vector of the initial velocity \mathbf{v} and the vector of the local normal to the specimen surface \mathbf{n} . The total number of the BSE emitted per second into the entire halfspace is

$$N = \frac{I_p}{e\pi} \int_0^1 F(\epsilon) \int_0^{2\pi} \int_0^{\pi/2} \cos\Omega \cos\Omega \sin\alpha_i d\alpha_i d\beta_i d\epsilon \quad (2)$$

The BSE signal from the semiconductor detector is not directly given by the number of BSE collected on the detector, but by the number of electron-hole pairs produced by the impinging electrons in the active area of the detector. This number S is energy-dependent; for our detector we can write with a good approximation

$$S(\epsilon) = \frac{E_p}{E_d} \epsilon \quad (3)$$

where E_d represents the energy necessary for one electron-hole pair, $E_d = 3.3$ eV. Combining (3) with (1), we have for the BSE signal

$$dN(\epsilon, \alpha_i, \beta_i) = \frac{I_p}{e\pi} S(\epsilon) F(\epsilon) \cos\Omega \sin\alpha_i d\alpha_i d\beta_i d\epsilon \quad (4)$$

In the classical arrangement of the SEM, the BSE show straight line trajectories. The BSE signal can be found by integration of (4) not over the entire halfspace, but over only that part of the solid angle above the specimen covered by the surface of the detector.

The curves in Fig.7 and Fig.8 illustrate that the position of the BSE in the detector plane is not a simple function of the initial velocity of the BSE at the specimen so we have no explicit expression for the integration region of the angles α_i and β_i . The only way out is to integrate over the entire halfspace as in (2), but then to add to the value of the integral only the contribution of those electrons, which satisfy the following two conditions:

1. they are able to leave the specimen (i.e. the condition) $-\frac{\pi}{2} < \Omega < \frac{\pi}{2}$
2. they impinge onto the detector (or onto a chosen segment of the detector) after passing through the magnetic field (i.e. the condition that the trajectory intersects the detector plane in the prescribed region).

We have mentioned that the trajectories are functions of the energy and that the backscattered electron energy spectrum is very broad. Therefore we must consider a real energy distribution for the calculation of the BSE contrast. We used the experimental curves of Kulenkampf and Spyra (given in the review article of Robinson, 1985) and approximated these curves by a suitable distribution function

$$F(\epsilon) = \eta_0 \frac{\sqrt{1 - \epsilon_m^2}}{\arctg \frac{1 + \epsilon_m}{1 - \epsilon_m}} \frac{1}{\epsilon^2 - 2\epsilon\epsilon_m + 1} \quad (5)$$

where ϵ is the relative energy, ϵ_m gives the position of the maxima of the energy distribution and η_0 is the backscattering coefficient for normal incidence. The parameters ϵ_m and η_0 depend on the atomic number.

References

Bode M, Reimer L. (1985). Detector strategy for a single-polepiece lens. *Scanning* 7, 125-133.

Delong A, Drahoš V, Kolařík V, Lenc M, Hladil K, Šálek R. (1978). A scanning electron microscope with a field emission gun (in Czech). *Slaboproudý obzor* 39, 443-449.

Hejna J, Reimer L. (1987). Backscattered electron multidetector system for improved quantitative topographic contrast. *Scanning* 9, 162-172.

Hill R, Smith KCA. (1982). The single-polepiece lens as a scanning electron microscope objective. *Scanning Electron Microsc. 1982; II*: 465-471.

Kruit P, Dubbeldam L. (1987). An E-beam tester with dispersive secondary electron energy analyser. *Scanning Microsc.* 1, 1641-1646.

Lenc M, Müllerová I. (1988). Efficient collection of BSE with single-polepiece lens. *Proceedings EUREM 88, York, England, I., IOP Publishing Ltd. Bristol, 117-118.*

Mulvey T. (1985). Magnetic electron lenses II, in *Electron Optical Systems, SEM Inc., AMF O'Hare (Chicago), 15-27.*

Oatley CW. (1983). Electron currents in the specimen chamber of a scanning electron microscope. *J. Phys. E: Sci. Instrum.* 16, 308-312.

Reimer L, Riepenhausen M, Tollkamp C. (1984). Detector strategy for improvement of image contrast analogous to light illumination. *Scanning* 6, 155-167.

Reimer L, Riepenhausen M. (1985). Detector strategy for secondary and backscattered electrons using multiple detector system. *Scanning* 7, 221-238.

Robinson VNE. (1980). Imaging with back-scattered electrons in a scanning electron microscope. *Scanning* 3, 15-26.

Robinson VNE. (1985). Electron detectors used for imaging in the scanning electron microscope, in *Electron Optical Systems, SEM Inc., AMF O'Hare (Chicago), 187-195.*

Discussion with Reviewers

O. Wells: Mention should be made of the paper by Tamura et al. (1980) describing a high resolution SEM using a snorkel lens of the sort used here. This predates the Hill and Smith (1982) reference cited here. It worries me that these authors use an upper magnetic shield to confine the magnetic field from the snorkel lens. This shield now acts as an upper polepiece, and I would have thought that a very close mechanical tolerance would be required---see, for example, the way in which Tamura et al. (1980) have an accurately machined polepiece in this position. Would the authors comment on this? What spatial resolution have they achieved?

Authors: The paper by Tamura et al. (1980) was not mentioned in our paper because we do not consider the lens they used single-polepiece, but unsymmetrical with a large gap. This leads to quite a different sensitivity to the misalignment of the upper polepiece. We

compared the influence of the mechanical deviation of the diameter of the "upper" polepiece D and of the distance between the "single" and "upper" polepieces S on the basic optical parameters for Tamura's geometry, see Fig.14 and Table 2a, and for our geometry, see Fig.5 and Table 2b.

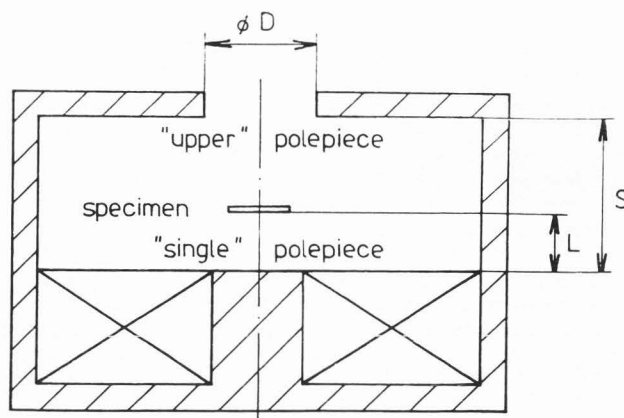


Fig. 14: The geometry of Tamura's snorkel lens. D - the diameter of the bore of the upper polepiece, L - the working distance and S - the distance between the "single" and "upper" polepieces.

Table 2: Electron optical parameters of Tamura's geometry (a) and our geometry (b) for an object at infinity. f , C_s , C_c are focal length, spherical and chromatic aberration coefficients in mm, respectively. The changes of geometry in mm are defined in Fig.14. The first line stands for the basic dimension.

(a)					
D	S	L	f	C_s	C_c
20	22	11	7.467	4.1	5.3
20	23	11	7.901	4.5	5.6
22	22	11	7.703	4.1	5.4

(b)					
D	S	L	f	C_s	C_c
24	80	5	14.007	4.0	8.4
24	85	5	13.957	4.0	8.4
34	80	5	14.000	4.0	8.4

The spatial resolution in our experimental column is limited by a low magnification of a telescopic system consisting of a condenser lens ($f \sim 70$ mm) and a single polepiece lens ($f \sim 14$ mm). With the gun cross-over of about $0.1 \mu\text{m}$ it gives 20 nm spot diameter, which is much higher than the aberration contribution at 15 keV primary beam energy.

O. Wells: There are, of course, two ways in which a solid specimen in the SEM can be immersed in a high magnetic field to reduce the aberrations and so improve the resolution. Mulvey's idea with the single polepiece lens is described here. The other way which has been implemented commercially for many years in both TEMs and STEMs manufactured by JEOL, ISI, VG, Hitachi and others is to mount the specimen between the polepieces of a condenser-objective lens of the sort that has been standard for many years in the TEM. Can the authors tell us how the aberrations (and therefore the resolution) compare in these two approaches?

Authors: We can only repeat reviewer's conclusions concerning snorkel lens: "Compared with the condenser-objective polepiece assembly, it offers more space for inserting large non-magnetic specimens and collectors, but the aberrations are somewhat worse (especially the chromatic aberrations)" (Munro and Wells, 1976). There are some other remarkable properties of the single-polepiece lens: a) it can be easily situated outside the vacuum, b) the ratio C_s/f is very low for the single polepiece lens, c) there is no steep decrease in flux density $B(z)$ and thus the approximation of the moving objective lens condition for the in-lens deflection field $D(z) = -i/2 B'(z)$ can be made for larger values of pre-deflection c .

I. Mulvey: Figure 5 shows a cross-section of the single-polepiece lens. Is there any special reason for providing an axial bore in this lens, since the electrons are brought to a focus before they reach the polepiece?

Authors: The bore in the single-polepiece lens does not influence the optical properties of the lens or the collection of BSE, but it concentrates the maximum of the focusing field on the specimen position, and this allows the approximation of the moving objective lens condition. The free space under the specimen can be utilized for a semiconductor detector of transmitted electrons.

O. Wells: Munro and Wells (1976) calculated the trajectories of BSE in a condenser-objective lens using a program in which the off-axis fields are calculated by relaxation over a mesh. How does the method of calculation you used here compare with Munro and Wells (1976)?

Authors: Our method of calculation makes use of an analytical expression for the flux density components, which is an exact solution of the Maxwell equations in vacuum, giving the Glaser field on the optical axis. The main advantage is that it provides smooth values for the calculation of the Lorentz force at any point, where the trajectory is calculated. On the other hand,

when the trajectory approaches a magnetic material (e.g. polepiece), our analytical expression does not correspond to the true flux density distribution any longer. It is not the case of a single-polepiece lens.

In the future we are going to use the same method as Munro did, with two important changes a) there will be a sufficiently smooth and simple interpolation of values at nodal points obtained by the finite element method (FEM), b) vector potential will be used as it gives more accurate results near the optical axis and it is possible to check the accuracy of the trajectory calculation not only by conservation of energy, but also by conservation of angular momentum.

F. Hasselbach: From your Fig.11 I conclude that for certain excitations of the single-polepiece lens a focused image of the specimen (more or less blurred by the aberrations) is formed in or near the detector plane. Do you think that this interpretation is valid or not? Would it be possible to prove this positioning a photographic plate in this plane during a scan of the whole specimen surface?

Authors: Yes, there is a focused specimen image in the detector plane for a certain excitation of the lens. The image is blurred mainly by the large energy width of the BSE spectrum. The proposed experiment with an energy filter in front of the detector (photographic plate) would be very interesting. The filter can serve also as an exposure shutter. We shall perform such an experiment in future.

F. Hasselbach: In your conclusions you mention a modification of an idea of VAIL. Could you please give a short description of this idea.

Authors: General information on our modification of the VAIL idea can be found in the paper Kolařík et al. (1989).

F. Hasselbach: A very interesting extension of your "imaging BSE" detector would be the possibility to apply to the specimen a negative potential of about 1 kV less than the accelerating potential of the scanning beam. In other words to convert your 15 keV SEM into a decelerating low voltage SEM. By switching on this negative voltage the secondary electrons will be accelerated, form an image and may be detected in similar manner as your BSE's. The aberrations of such a decelerating field (for the primary beam) are small according to an early theoretical and experimental study of Pease (1967), i.e. the spot size of the primary beam on the specimen surface is not enlarged drastically by this additional electrostatic lens field. All advantages of your detector system would be extended to the secondary electron image. Do you think that this idea can be realized easily?

Authors: The idea can be realized easily, and we are thinking about this even in connection with the low voltage scanning electron microscope. As Bauer (1985) has shown, the combination of the decelerating quasi-homogeneous electric field and electrostatic lens enables one to obtain a very good resolution even for final energy below 100 eV. So we expect the combination of the

decelerating field with the magnetic single-polepiece lens will perhaps give better results, and we plan this experiment in the near future.

I. Mulvey: You say that the work was carried out in the Tesla BS 350 UHV SEM. Surely this required extensive instrumental modifications? Could you outline briefly what is necessary if one wished to try out this method?

Authors: 1. It is necessary to ensure free space under the bottom of the SEM chamber. 2. To locate a single polepiece lens sufficiently far from SEM iron parts which could negatively affect optical properties of the lens. 3. It seems that a conventional manipulator of the specimen will not be suitable. For basic experiments, a specimen can be located directly on the polepiece. For more complicated experiments a construction of a new manipulator is necessary. Its movement mechanisms should not influence the magnetic field of the single-polepiece lens and should allow movement of the specimen sufficiently near to the polepiece. 4. The detector of SE must be located in the space of a sufficiently low value of the field of the single-polepiece lens.

Additional References

Bauer E. (1985). The resolution of the low energy electron reflection microscope. *Ultramicroscopy* 17, 51-56.

Kolařík V, Müllerová I, Lenc M. (1989). SEM with the single-polepiece objective lens. *Scanning Microsc.* (in press)

Munro E, Wells OC. (1976). Some comments on the design of magnetic lenses for the scanning electron microscope. *Scanning Electron Microsc.* 1976; I: 27-36.

Pease RFW. (1967). Low Voltage Scanning Electron Microscopy, Record of IEEE 9th Symposium on Electron, Ion and Laser Beam Technology, Berkeley 1967, RFW. Pease (ed.), San Francisco Press, 176-187.

Tamura N, Saito H, Ohyama J, Aihara R, Kabaya A. (1980). Field emission SEM using strongly excited objective lens. 38th Ann. Proc. Amer. Soc. Electron Microscopy, San Francisco, 1980. GW Bailey (ed.), Claitors Publ. Div. Baton Rouge, Louisiana, 68-69.